Generalizing the trapezoidal rule in the complex plane

Bengt Fornberg *
Department of Applied Mathematics, University of Colorado, Boulder, CO 80309, USA

May 22, 2020

Abstract

In computational contexts, analytic functions are often best represented by grid-based function values in the complex plane. For integrating periodic functions, the spectrally accurate trapezoidal rule (TR) then becomes a natural choice, due to both accuracy and simplicity. The two key present observations are (i) The accuracy of TR in the periodic case can be greatly increased (doubling or tripling the number of correct digits) by using function values also along grid lines adjacent to the line of integration, and (ii) A recently developed end correction strategy for finite interval integrations applies just as well when using these enhanced TR schemes.

Keywords: Euler-Maclaurin, trapezoidal rule, contour integrals, equispaced grids, hexagonal grid.
AMS classification codes: Primary: 65B15, 65E05; Secondary: 30-04.

1 Introduction

There are two main scenarios when approximating contour integrals in the complex plane:

i. The function to integrate can be obtained at roughly equal cost for arbitrary spatial locations, and

ii. Function values are available primarily on an equispaced grid in the complex plane.[1]

In case (i), a commonly used option is Gaussian quadrature[2], either applied directly over the whole interval of interest, or combined with adaptive interval partitioning. Conformal (and other) mappings may be applied both for straightening curved integration paths (such as Hankel contours) and to improve the resolution in critical places.

* *Email*: fornberg@colorado.edu

[1] If an analytic functions is somewhat costly to evaluate, it may be desirable to pay a one-time cost of evaluating over a grid and then re-use this data for multiple purposes, such as for graphical displays (e.g., [7, 12]) and, as focused on here, for highly accurate contour integrations (assuming some vicinity of the integration paths to be free of singularities). In some cases, the fastest evaluation method for the function is naturally grid based (e.g. the Painlevé functions [8]).

[2] The present application is atypical in that Clenshaw-Curtis requires roughly twice as many evaluation points as Gaussian quadrature for matching accuracies; c.f., [10] and the discussion in Section 4.2 of [4].

This present study focuses on case (ii). With equispaced data available, the trapezoidal rule (TR) is a natural option to consider. It is well known to be spectrally accurate for smooth periodic data [11].[3] In finite interval non-periodic situations, the Euler-Maclaurin (EM) formula provides opportunities for highly accurate end corrections. These may be carried out using analytic derivatives, or (requiring no analytic differentiations) with finite differences (FD) approximations. Recent articles analyze the cases when these (equi-spaced) FD stencils use data points only within the interval [6], extend only in the direction of the line of integration [5], or extend over a region of the complex plane surrounding each end point [4].

Previous test cases (e.g., Figure 5 in [4]) showed that, in spite of being spectrally accurate (as opposed to the finite order accuracy of FD-type corrections), the TR integral along the interior of the line segment nevertheless often becomes the dominant error source. This motivated the present work, as it raised questions such as:

i. Can the periodic TR be improved on by incorporating data not just along the actual line of integration, but also from parallel grid lines adjacent to it, and

ii. If so, can also such improved accuracy periodic TR schemes be combined with effective 'end corrections' for use in non-periodic cases.

These two issues are addressed in Sections 2 and 3, followed by more extensive numerical tests in Section 4. This in turn is followed by Conclusions, References, and an Appendix.

2 The periodic TR in the complex plane

The TR applied to a periodic function uses function values at equispaced grid points along the line of integration. If the grid spacing is too large for providing the desired accuracy, the two most often considered options are (i) reduce the grid spacing, and (ii) supplement function values with derivative values and use a Hermite-based TR generalization [2]. Yet another option is to utilize (presumably already available) function values also from adjacent grid lines.[4] We will next analyze this third option in the two cases of equispaced Cartesian and hexagonal grids. An alternative approach to the one described next for deriving such multi-line TR formulas is given in the Appendix, providing a supplementary perspective by using contour integration instead of Fourier series expansion.

2.1 Equispaced Cartesian grid

Let $z = x + i\,y$ and $f(z)$ be 2π-periodic and analytic in a strip surrounding the x-axis. This interval is discretized using N nodes in the x-direction, i.e. with step size $h = 2\pi/N$. In the Fourier expansion

$$f(z) = \sum_{k=-\infty}^{\infty} c_k e^{ikz},$$

[3] First observed by Poisson in the 1820's [9]

[4] Although many papers discuss and give error estimates for the periodic TR, there seem to be few – if any – previous references on utilizing this type of supplementary information for improving the accuracy. A somewhat related procedure was used in [3] for approximating derivatives / Taylor coefficients (c.f., its equations (5) - (9)).

	Cartesian grid	Hexagonal grid
Common factor	$\dfrac{1}{(2\sinh(\pi))^4(2\cosh(\pi))^2}$	$\dfrac{\left(2\sinh\left(\frac{\sqrt{3}\pi}{2}\right)\right)^2}{\left(2\sinh(\sqrt{3}\pi)\right)^4}$
Weights	1 $-2\left(\cosh(2\pi)+\cosh(4\pi)\right)$ $2\left(1+\cosh(2\pi)+\cosh(6\pi)\right)$ $-2\left(\cosh(2\pi)+\cosh(4\pi)\right)$ 1	-1 $-2\left(\cosh(\sqrt{3}\pi)-2\cosh(2\sqrt{3}\pi)\right)$ $2\left(-1+\cosh(\sqrt{3}\pi)+\cosh(3\sqrt{3}\pi)\right)$ $-2\left(\cosh(\sqrt{3}\pi)-2\cosh(2\sqrt{3}\pi)\right)$ -1

Table 1: Weights to use in the 5-line periodic TR generalizations.

the coefficients c_k will be decaying (at least) exponentially fast with increasing $|k|$. Due to *aliasing*, modes for which k differs by a multiple of N are indistinguishable on the grid. TR applied along the x-axis will thus return the result

$$T_0 = 2\pi\left\{\ldots + c_{-2N} + c_{-N} + c_0 + c_{+N} + c_{+2N} + \ldots\right\}. \tag{1}$$

Here, $2\pi c_0$ is the exact value for the integral, and the remaining terms represent errors. Applying the TR along the grid lines just below and above return

$$T_- = 2\pi\left\{\ldots + c_{-2N}e^{-4\pi} + c_{-N}e^{-2\pi} + c_0 + c_{+N}e^{2\pi} + c_{+2N}e^{4\pi} + \ldots\right\} \tag{2}$$

and

$$T_+ = 2\pi\left\{\ldots + c_{-2N}e^{4\pi} + c_{-N}e^{2\pi} + c_0 + c_{+N}e^{-2\pi} + c_{+2N}e^{-4\pi} + \ldots\right\}. \tag{3}$$

The three results can be combined to eliminate the leading errors due the $c_{\pm N}$ terms, giving

$$T = \frac{1}{(2\sinh\pi)^2}\left\{-T_- + 2\cosh(2\pi)\,T_0 - T_+\right\} = 2\pi c_0 + O(c_{\pm 2N}). \tag{4}$$

These coefficients for $\{T_-, T_0, T_+\}$ are approximately $\{-0.001874,\ 1.00375, -0.001874\}$. The regular TR term T_0 strongly dominates in (4). Nevertheless, T will have roughly double the number of correct digits compared to the (already spectrally accurate) T_0 result. This 3-line case can readily be generalized to using still more lines. Using 5 lines, also the $c_{\pm 2N}$ terms can be eliminated, giving weights that differ little from the 3-line case: $\{6.5\cdot10^{-9}, -0.001878,\ 1.00376, -0.001878,\ 6.5\cdot10^{-9}\}$. Exact values for these coefficients (as well as for the 5-line hexagonal counterpart discussed next) are given in Table 1.[5]

2.2 Equispaced hexagonal grid

As in the Cartesian case, T_0 is given by (1), but then

$$T_- = 2\pi\left\{\ldots + c_{-2N}e^{-2\sqrt{3}\pi} - c_{-N}e^{-\sqrt{3}\pi} + c_0 - c_{+N}e^{\sqrt{3}\pi} + c_{+2N}e^{2\sqrt{3}\pi} + \ldots\right\}, \tag{5}$$

and

$$T_+ = 2\pi\left\{\ldots + c_{-2N}e^{2\sqrt{3}\pi} - c_{-N}e^{\sqrt{3}\pi} + c_0 - c_{+N}e^{-\sqrt{3}\pi} + c_{+2N}e^{-2\sqrt{3}\pi} + \ldots\right\}. \tag{6}$$

[5]Repeated application of Birkhoff-Young type formulas (first introduced in [1]) also produce multi-line TR-like formulas in the periodic case. However, as noted in [4], Section 4.3, their weights become such that they reduce rather than improve the accuracy compared to the regular TR.

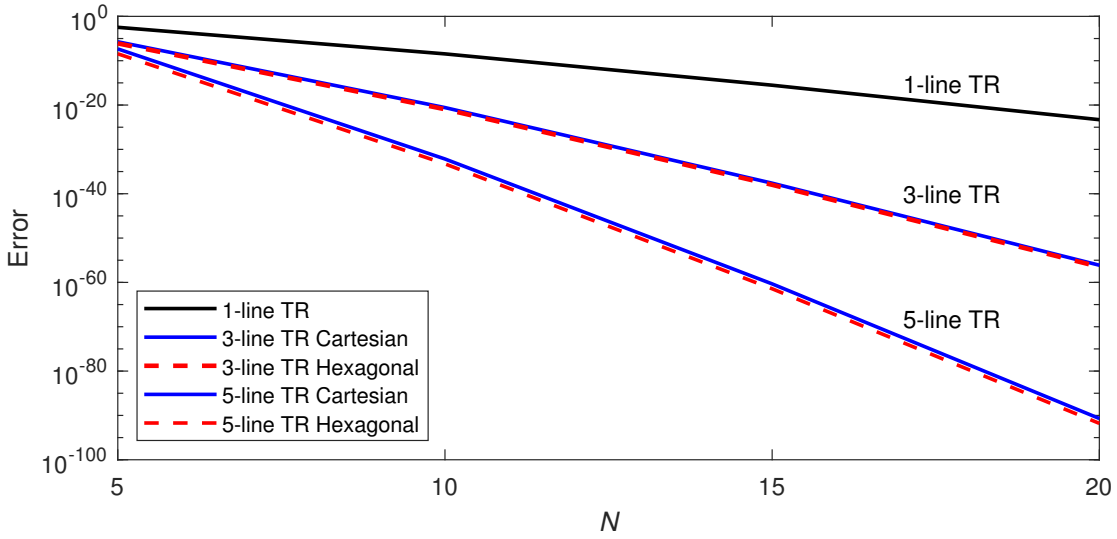

Figure 1: Log-linear display of the error approximating (8) with the TR and its 3- and 5-line extensions.

The combination that eliminates the leading errors (again caused by the $c_{\pm N}$ terms) is now

$$T = \frac{1}{\left(2\cosh\left(\frac{\sqrt{3}\pi}{2}\right)\right)^2}\left\{T_- + 2\cosh(\sqrt{3}\pi)\,T_0 + T_+\right\} = 2\pi c_0 + O(c_{\pm 2N}). \tag{7}$$

Numerically, these coefficients for $\{T_-, T_0, T_+\}$ are approximately $\{0.0043,\ 0.9914,\ 0.0043\}$ (with the approach again readily extendable to cases using still more grid lines).

2.3 Numerical illustration of periodic multi-line TR generalizations

To illustrate the accuracies gained over TR by the 3-line formulas (4), (7), and their 5-line counterparts given in Table 1, we consider the test problem

$$\int_0^{2\pi} e^{\cos x} dx = 2\pi I_0(1) \approx 7.9549265210, \tag{8}$$

where I denotes the I-Bessel function. Asymptotic analysis will show that $c_k \sim 2^{-|k|}/|k|!$, i.e., a somewhat faster than exponential decay (to be expected, since $e^{\cos z}$ is an entire function).[6] Figure 1 shows that including data from adjacent lines is roughly equally effective on both grid types, To reach double precision (10^{-16}) accuracy, TR needs in this case $N \approx 16$ whereas, in the 5-line cases, $N \approx 7$ suffices. For quad precision (10^{-34}), the corresponding numbers are $N \approx 28$ vs. $N \approx 10$.[7]

The accuracy of the multi-line TR versions when poles are present near to the line of integration is discussed later in Section 4.3.

[6] c.f., [13], Example 5, and [7], page 353.

[7] We recall the assumption that grid-based data is more economically available than 'fresh' function evaluations. If not, it would be more cost effective to double and triple the number of nodes in the 1-line TR than to apply the 3-line and 5-line TR versions, respectively.

3 End corrections for non-periodic cases

The Euler-Maclaurin formula is described in Section 3.1. As was shown in [4], this formula provides a convenient means for obtaining FD-type end correction weights in non-periodic TR cases. We have above generalized the periodic TR to the use of multiple lines, and wish again to find high-order end corrections. Rather than again using the EM formula as the starting point, it turns out to be easier to take one step back, and instead start with one (of many) ways used to derive the EM formula. This is carried out in Sections 3.2 and 3.3 for the Cartesian and hexagonal grid cases, respectively.

3.1 The Euler-Maclaurin formula

In the case of a semi-infinite integration interval $0 \le z < \infty$, with grid spacing h, the Euler-Maclaurin (EM) formula becomes

$$\begin{aligned}\int_0^\infty f(x)dx &= \left\{ h\sum_{k=0}^{\infty} f(kh) - \frac{h}{2}f(0) \right\} + \frac{h^2}{12}f^{(1)}(0) - \frac{h^4}{720}f^{(3)}(0) + \frac{h^6}{30240}f^{(5)}(0) - + \dots \qquad (9)\\ &= \left\{ h\sum_{k=0}^{\infty} f(kh) - \frac{h}{2}f(0) \right\} + \sum_{k=1}^{\infty} \frac{h^{2k}B_{2k}}{(2k)!}f^{(2k-1)}(0).\end{aligned}$$

Here the B_{2k} are the even order Bernoulli numbers. The sum in the curly brackets is the standard (one-line) TR. In this one-sided case, we can write the weights in the TR part as

$$h\left\{ \tfrac{1}{2}, \quad 1, \quad 1, \quad 1, \quad 1, \quad \dots \right\}. \qquad (10)$$

One approach for deriving (9) is to consider the difference between the exact integral $\int_0^\infty f(z)dz$ and its TR approximation for the test function $f(\xi, z) = e^{-z\,\xi}$. For the approximation (10) (with $h = 1$), this difference becomes

$$g(\xi) = \left\{ \int_0^\infty e^{-z\xi}dz \right\} - \left\{ \frac{1}{2} + \sum_{k=1}^{\infty} e^{-k\xi} \right\} = \left\{ \frac{1}{\xi} \right\} - \left\{ \frac{1}{2}\coth\left(\frac{\xi}{2}\right) \right\}. \qquad (11)$$

This is an odd function in ξ, with $\xi = 0$ a removable singularity. Noting that $\frac{d^k}{dz^k}f(\xi, z)\Big|_{z=0} = (-\xi)^k$, Taylor expanding $g(\xi)$ gives the coefficients in (9). Several cases of FD-type end correction weights based on these EM coefficients were given in closed form in [4].

3.2 Cartesian grid

In view of (4) and in the style of (10), the one-sided 3-line TR stencils we wish to end correct can be written as

$$h\,\frac{1}{(2\sinh\pi)^2}\left\{ \begin{bmatrix} [\ \ -1\ \ ] & \cdot\{ & \tfrac{1}{2}, & 1, & 1, & 1, & \dots\} \\ [2\cosh 2\pi] & \cdot\{ & \tfrac{1}{2}, & 1, & 1, & 1, & \dots\} \\ [\ \ -1\ \ ] & \cdot\{ & \tfrac{1}{2}, & 1, & 1, & 1, & \dots\} \end{bmatrix} \right\}. \qquad (12)$$

The counterpart to (11) becomes now

$$g(\xi) = \left\{ \frac{1}{\xi} \right\} - \left\{ \frac{\cosh 2\pi - \cos\xi}{(2\sinh\pi)^2}\coth\left(\frac{\xi}{2}\right) \right\}, \qquad (13)$$

again an odd function in ξ, regular at $\xi = 0$. Instead of proceeding via EM-type expansion coefficients for odd order derivatives as an intermediate step[8], we can aim more directly for the weights in a correction stencil. Let this be of size 5×5, centered at the origin of the complex z-plane, with weights

$$\begin{bmatrix} a_1 & a_2 & a_3 & a_4 & a_5 \\ a_6 & a_7 & a_8 & a_9 & a_{10} \\ a_{11} & a_{12} & a_{13} & a_{14} & a_{15} \\ a_{16} & a_{17} & a_{18} & a_{19} & a_{20} \\ a_{21} & a_{22} & a_{23} & a_{24} & a_{25} \end{bmatrix} . \tag{14}$$

Matching Taylor expansion coefficients between (13) and (14) (also applied to $e^{-z\xi}$) up through $O(\xi^{24})$ gives 25 linear relations for the 25 coefficients in (14). This procedure can be implemented in very few lines of code in either symbolic or numerical languages. For example in Mathematica:[9]

```
z = Flatten[Table[i - ⅈ j, {j, -2, 2}, {i, -2, 2}]];
S = 1/ξ - ((Cosh[2 π] - Cos[ξ])/(2 Sinh[π])^2 Coth[ξ/2]) - Sum[c[k] e^(-z[[k]] ξ), {k, 1, 25}];
NSolve[LogicalExpand[Series[S, {ξ, 0, 24}] == 0], 30]
```

The calculations described below used this approach, but were instead implemented in MATLAB using its symbolic toolbox and the Advanpix Multiprecision Package[10].

The correction weights for this 3-line TR extension case feature exactly the same symmetry pattern as in the TR case described in [4],

$-c_8 + ic_9$	$-c_{10} + ic_{11}$	ic_{12}	$c_{10} + ic_{11}$	$c_8 + ic_9$
$-c_6 + ic_7$	$-c_2 + ic_3$	ic_4	$c_2 + ic_3$	$c_6 + ic_7$
$-c_5$	$-c_1$	0	c_1	c_5
$-c_6 - ic_7$	$-c_2 - ic_3$	$-ic_4$	$c_2 - ic_3$	$c_6 - ic_7$
$-c_8 - ic_9$	$-c_{10} - ic_{11}$	$-ic_{12}$	$c_{10} - ic_{11}$	$c_8 - ic_9$

making it sufficient to give values in the first quadrant. With errors less that $\frac{1}{2}10^{-20}$, these 12 coefficients are:

$$\begin{aligned}
c_1 &\approx 0.01584538613124865210 , & c_7 &\approx -0.00001086091533534879 , \\
c_2 &\approx 0.00196114131223055449 , & c_8 &\approx -0.00000017592393798095 , \\
c_3 &\approx -0.00179604028335645052 , & c_9 &\approx 0.00000017192139599287 , \\
c_4 &\approx -0.01936320425382213082 , & c_{10} &\approx 0.00001143418528633658 , \\
c_5 &\approx -0.00006132067581641948 , & c_{11} &\approx -0.00001107294056928483 , \\
c_6 &\approx 0.00001116130210519658 , & c_{12} &\approx 0.00006428142367113119 .
\end{aligned}$$

[8] as was done in [4]

[9] The last parameter in the NSolve statement specifies the precision (number of decimal digits) to be used in this calculation of the coefficients.

[10] Advanpix, Multiprecision Computing Toolbox for MATLAB , http://www.advanpix.com/, Advanpix LLC., Yokohama, Japan.

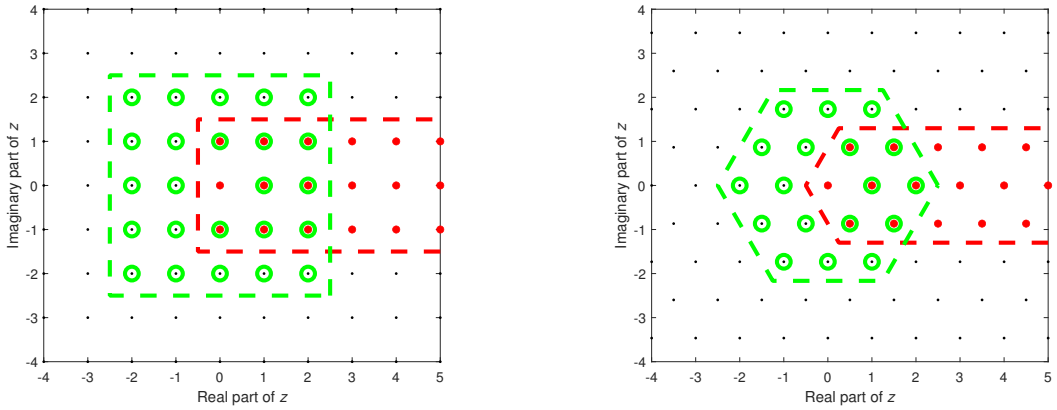

(a) 5×5 Cartesian correction stencil (b) 19 node hexagonal correction stencil

Figure 2: Illustrations of the correction stencils in the 3-line TR versions, on a Cartesian and a hexagonal grid, respectively. In both cases, the center point is not marked with a green circle, since its coefficient is zero.

Also these weights are very small compared to those of the regular TR method. Figure 2 (a) illustrates schematically this Cartesian grid end correction, with part (b) showing the 19 node hexagonal counterpart to be derived next.

In the case of end correcting the 5-line TR extension (as given to the left in Table 1), the $g(\xi)$-function becomes

$$g(\xi) = \left\{ \frac{1}{\xi} \right\} - \left\{ \left(\frac{1 + \cosh(2\pi) + \cosh(6\pi) + \cos(2\xi)}{(2\cosh(\pi))^2} + (1 - 2\cosh(2\pi))\cos(\xi) \right) \frac{\coth\left(\frac{\xi}{2}\right)}{(2\sinh(\pi))^4} \right\}.$$

3.3 Hexagonal grid

The counterparts to (12) and (13) are now

$$h \, \frac{1}{\left(2\cosh\left(\frac{\sqrt{3}\pi}{2}\right)\right)^2} \left\{ \begin{bmatrix} 1 \end{bmatrix} \cdot \{ 1, \; 1, \; 1, \; 1, \ldots \} \atop \begin{bmatrix} 2\cosh(\sqrt{3}\pi) \end{bmatrix} \cdot \{ \tfrac{1}{2}, \; 1, \; 1, \; 1, \; \ldots \} \atop \begin{bmatrix} 1 \end{bmatrix} \cdot \{ 1, \; 1, \; 1, \; 1, \ldots \} \right\}, \tag{15}$$

and

$$g(\xi) = \left\{ \frac{1}{\xi} \right\} - \left\{ \frac{\cosh\left(\sqrt{3}\pi\right)\cosh\left(\frac{\xi}{2}\right) + \cos\left(\frac{\sqrt{3}}{2}\xi\right)}{(2\cosh\left(\frac{\sqrt{3}\pi}{2}\right))^2 \sinh\left(\frac{\xi}{2}\right)} \right\}. \tag{16}$$

This produces an end correction stencil with an equivalent symmetry pattern to the Cartesian case:

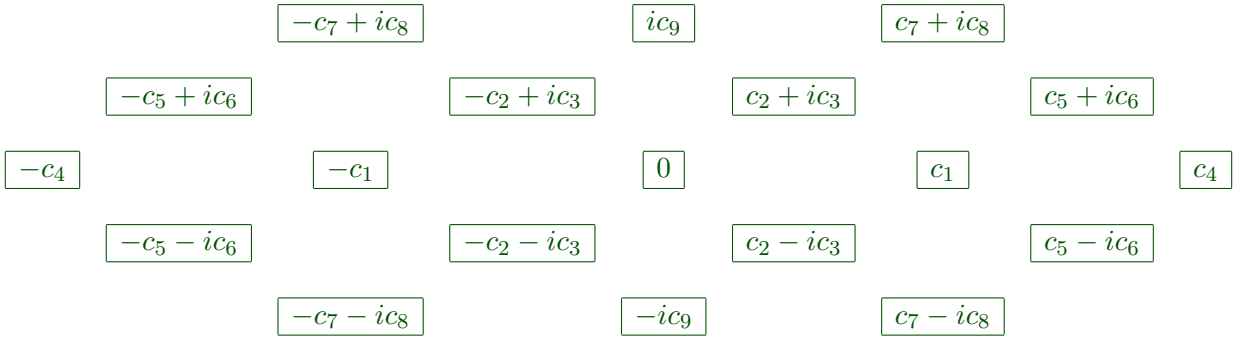

Numerically, these coefficients are

$$\begin{aligned}
c_1 &\approx 0.01218793670602685516\ , & c_6 &\approx -0.00009145928037900647\ ,\\
c_2 &\approx 0.00760486586506297724\ , & c_7 &\approx -0.00001637979980581665\ ,\\
c_3 &\approx -0.01091720972542147556\ , & c_8 &\approx 0.00002711120964812859\ ,\\
c_4 &\approx -0.00003075414473262889\ , & c_9 &\approx -0.00019964030657406958\ .\\
c_5 &\approx 0.00016687789689093499\ ,
\end{aligned}$$

The procedure in these Sections 3.2 and 3.3 generalizes immediately both to larger sized correction stencils (i.e., higher orders of accuracy) and to TR versions based on more lines.

When correcting at the end rather than at the start of an integration interval, the sign should be changed for all the correction weights (Cartesian and hexagonal).

4 Numerical tests

To simplify comparisons, we use the same test function as in [4]:

$$f(z) = \frac{2}{z-0.4\,(1+i)} - \frac{1}{z+0.4\,(1+i)} + \frac{1}{z+1.2-1.6i} - \frac{3}{z-1.3-2i}. \tag{17}$$

4.1 Comparison between present grid-based methods for two different closed paths

As in [4], we consider again the two closed paths illustrated in Figure 3:

1. The rectangular path with corners $z = \{1, 1+i, -1+i, -1\}$ (using a Cartesian grid), and
2. The equilateral triangular path with corners $z = \{1, i\sqrt{3}, -1\}$ (using a hexagonal grid),

and integrate around these in the positive direction. The analytic result becomes $\int_C f(z)dz = 4\pi i$ (since the only singularity inside the paths is the pole at $z = 0.4\,(1+i)$). For the two grid types, we use the 5×5 and 19-node correction stencils, respectively. In this latter case, Figure 4 shows the real and imaginary parts of $f(z)$ on a hexagonal $h = 0.1$-spaced grid, marking also the nodes utilized for the quadrature.[11]

[11] Figure 6 in [4] shows similarly the nodes used when integrating along the rectangle in the Cartesian node case.

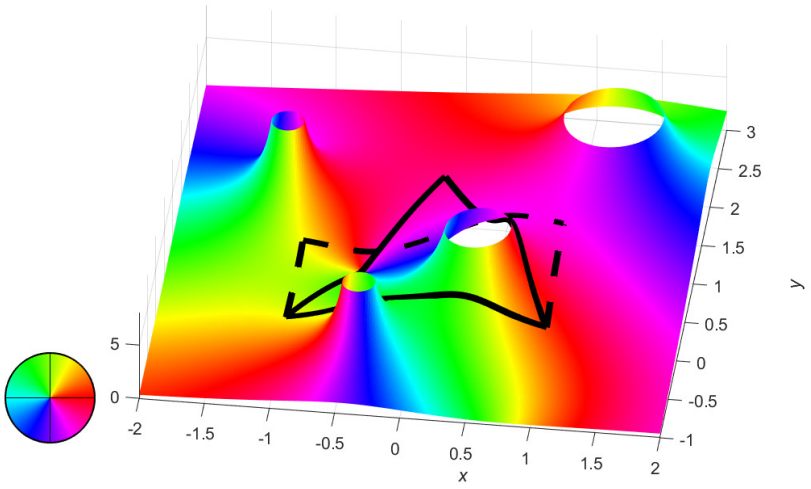

Figure 3: Magnitude and phase angle display of the test function (17) with the two integration paths marked over the magnitude surface.

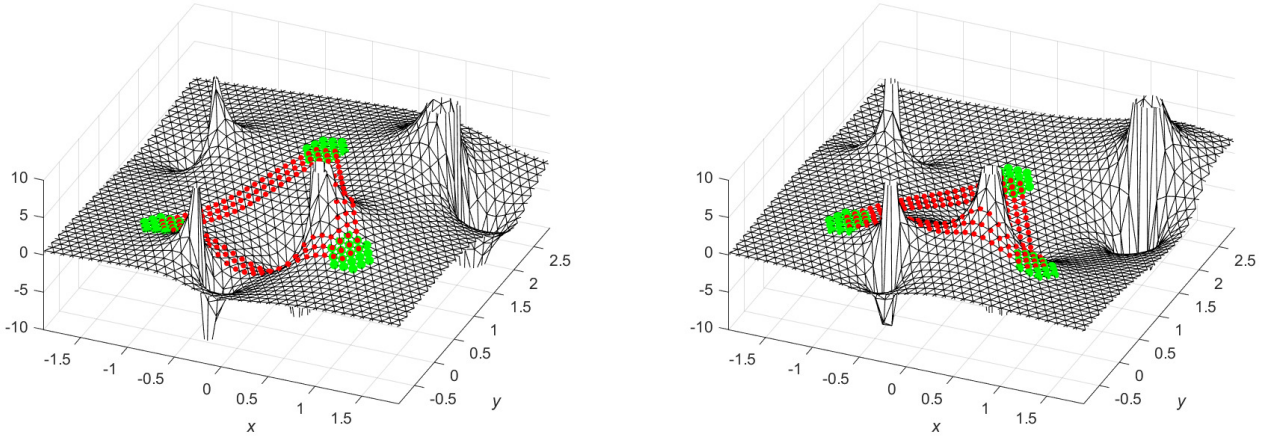

(a) Real part of $f(z)$

(b) Imaginary part of $f(z)$

Figure 4: Real and imaginary parts of $f(z)$ (as given by (17)) displayed on a hexagonal grid with spacing $h = 0.1$. The nodes used when integrating with the 3-line TR and 19-node end corrections are marked in red and green, respectively. As seen from the solid red curve in Figure 5, this displayed $h = 0.1$ resolution suffices for an accuracy of around 10^{-14}.

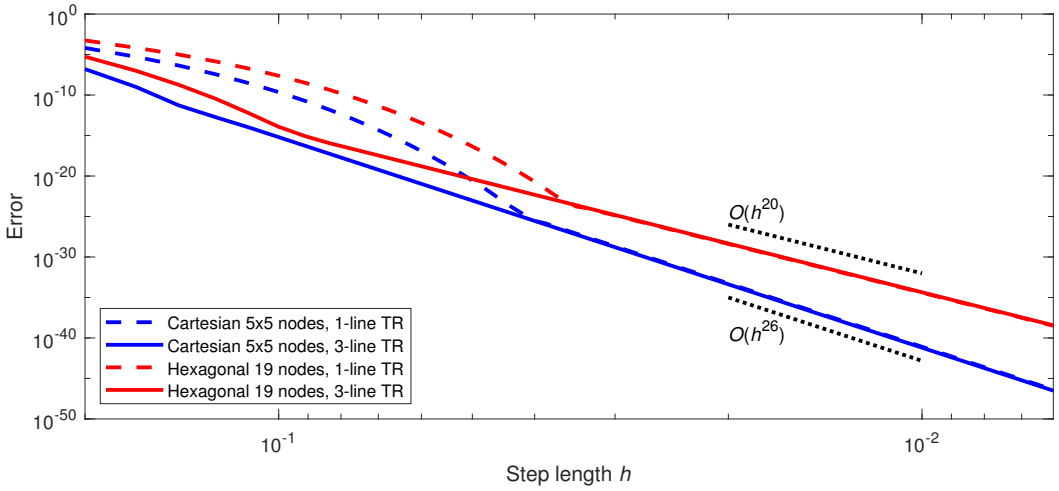

Figure 5: Log-log plot of the absolute error when using the four different quadrature implementations on their respective integration paths (rectangular in the Cartesian cases, and following an equilateral triangle in the hexagonal cases). The two dashed curves (1-line TR cases) match exactly the corresponding curves in Figure 5 in [4].

Figure 5 shows how the numerical errors in these quadratures decrease with the step size h on Cartesian and hexagonal equi-spaced grids. In the regular 1-line TR cases, there is a distinct transition point, after which the algebraic order errors from the ends of the segments become dominant. The slopes of these straight lines confirm the expected algebraic convergence orders of the end corrections.[12] We also see that, when changing from regular TR to the 3-line TR generalizations, errors in the (usually most important double precision range) become reduced by several orders of magnitude.

4.2 Test case where the corner errors are less significant

Rather than integrate $f(z)$, as defined in (17) around the closed contours as above, we use as the next test problem $\int_{-5}^{5} f(z)dz \approx 1.318423 + 4.417331i$.[13] To the left in Figure 6, TR errors dominate those from the ends while, to the right, we see the algebraic order errors from the ends. The accuracy gains seen when changing from the regular TR to its 3-line and 5-line TR enhancement are similar to those seen in Figure 1 (although now displayed in log-log form in order to match Figure 5 rather than log-linear as used in Figure 1).

4.3 Accuracy of the multi-line TR approximations for h large

There will obviously be a severe loss of accuracy if the grid step h is so large that there is a singularity in-between the lines of a multi-line TR approximation. However, Figures 5 and 6 show that the accuracy loss (relative to the 1-line TR) is minor, even when coming close too this extreme case.

[12] One higher than the number of nodes in the correction stencil.

[13] In Section 4.3 of [4], end corrected 1-line TR is compared against Gaussian and Clenshaw-Curtis quadratures for the test problem $\int_{-1}^{1} f(z)dz$.

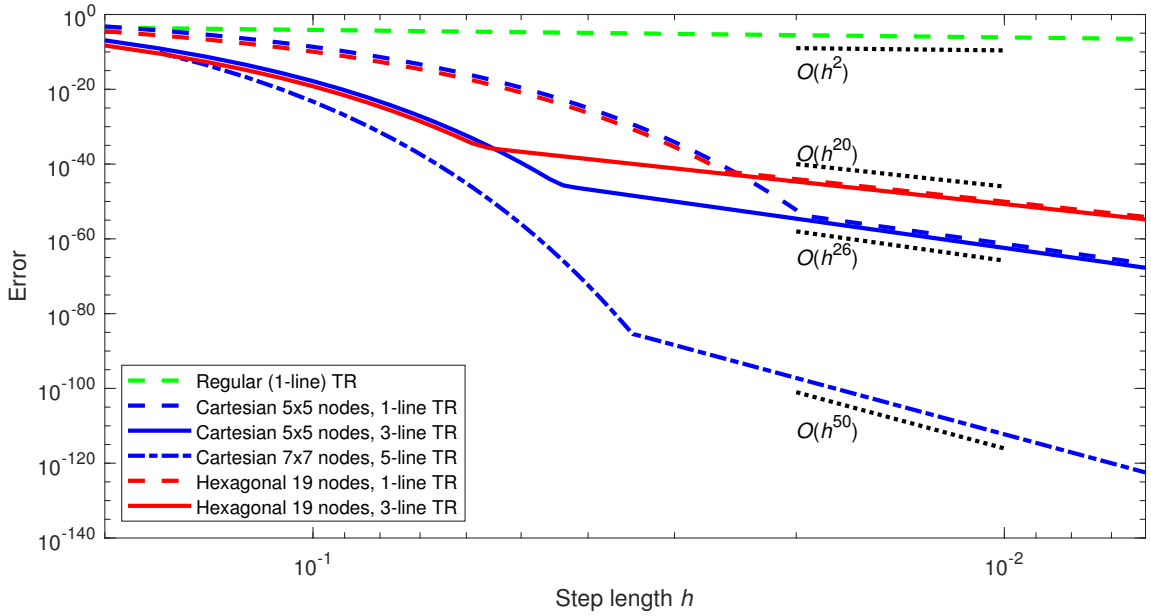

Figure 6: Log-log plot of the absolute error when using six different quadrature implementations applied to $\int_{-5}^{5} f(z)dz$, with $f(z)$ given in (17).

4.3.1 First test case: Triangular path (Section 4.1)

In the triangular path case, the distance from the upper right leg of the triangle to the nearest singularity is about 0.32. Both in the case of $h = 0.1$ (as illustrated in Figure 4) and for $h = 0.2$ (seen at the left edge of Figure 5), the 3-line TR approximation features roughly double the number of correct digits as the 1-line TR version. In other words, even with a pole only about $h/2$ distant from the outer line in the 3-line TR approximation, its accuracy advantage over 1-line TR is maintained.

4.3.2 Second test case: Straight line path (Section 4.2)

In this test, there are two (different strength) poles a distance of 0.4 from the line of integration. The left part of Figure 6 shows the pattern (double digit benefit of the 3-line TR vs. 1-line TR) to persist even with h as large as 0.2. Although the 5-line TR here also gave an acceptable result for $h = 0.2$, this was by lucky chance only. With both poles of the integrand and quadrature nodes at a distance of $2h = 0.4$ from the line of integration, there could have been a coincidence in location, with the approximation then evaluating to infinity. Soon after h has been decreased below 0.1, its advantage over the 3- and 1-line TR versions becomes similar to the singularity-free case illustrated in Figure 1.

5 Conclusions

Spectral convergence of the trapezoidal rule (TR) for periodic problems, and also the Euler-Maclaurin (EM) formula for TR 'end corrections' in cases of finite intervals[14] are both classical results. It was recently observed that, assuming the integrand to be analytic, the end corrections

[14] when expressed as derivatives of odd orders at the end point(s)

alternatively can be expressed very accurately as a linear combination of function values at grid points near to the interval's end points. With this as motivation, we have here first noted that the basic TR in the periodic case can be made far more accurate still by also using function values from grid lines adjacent to the line of integration. The second key observation is that the end correction approach for integrating along finite line segments carry over also to this case. These corrections are for numerical use most conveniently expressed as weights to apply at grid points near to the interval end points. The equispaced grid in the complex plane can here be either Cartesian or hexagonal. In both the periodic and in the finite interval cases, the formulas presented here generalize immediately to still higher levels of accuracy.

Discussions with André Weideman are gratefully acknowledged.

References

[1] G. Birkhoff and D. Young, *Numerical quadrature of analytic and harmonic functions*, J. Math. Physics **29** (1950), 217–221.

[2] C.R. Burne, *Derivative corrections to the trapezoidal rule*, arXiv (2018), 1808.04743v1 [math.NA].

[3] B. Fornberg, *Numerical differentiation of analytic functions*, ACM Trans. Math. Software **7** (1981), no. 4, 512–526.

[4] ———, *Contour integrals of analytic functions given on a grid in the complex plane*, IMA Journal of Num. Anal. (to appear) (2020).

[5] ———, *Euler-Maclaurin expansions without analytic derivatives*, submitted (2020).

[6] ———, *Improving the accuracy of the trapezoidal rule*, SIAM Review (to appear) (2020).

[7] B. Fornberg and C. Piret, *Complex Variables and Analytic Functions: An Illustrated Introduction*, SIAM, 2020.

[8] B. Fornberg and J.A.C. Weideman, *A numerical method for the Painlevé equations*, J. Comput. Phys. **230** (2011), 5957–5973.

[9] S.-D. Poisson, *Sur le calcul numérique des intégrales définies*, Mémoires de l'Académie Royale des Sciences de l'Institute de France **4** (1827), 571–602.

[10] L.N. Trefethen, *Is Gauss quadrature better than Clenshaw-Curtis?*, SIAM Review **50** (2008), no. 1, 67–87.

[11] L.N. Trefethen and J.A.C. Weideman, *The exponentially convergent trapezoidal rule*, SIAM Review **56** (2014), 384–458.

[12] E. Wegert, *Visual Complex Functions*, Birkhäuser, 2012.

[13] J.A.C. Weideman, *Numerical integration of periodic functions: A few examples*, Amer. Math. Monthly **109** (2002), 21–36.

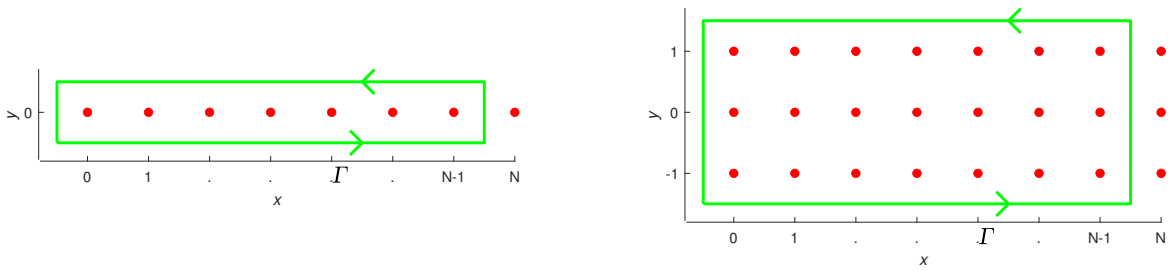

(a) Contour for 1-line TR.

(b) Contour for 3-line TR.

Figure 7: Contours and pole locations in the contour integration-based derivations of the periodic 1-line and 3-line TR methods.

6 Appendix: Derivation of multi-line periodic TR formulas by means of contour integration

For notational simplicity, we set $h = 1$ and let the problem be periodic over $0 \le x \le N$. With the path Γ illustrated in Figure 7 (a),

$$\frac{1}{2\pi i}\int_\Gamma f(z)\,\pi\cot\pi z\,dz = \left\{\begin{array}{c}\text{sum of resi-}\\ \text{dues inside } \Gamma\end{array}\right\} = \sum_{k=0}^{N-1} f(k) = \left\{\begin{array}{c}\text{TR result for}\\ \int_0^N f(x)dx\end{array}\right\}. \tag{18}$$

We next note:

1. The value of $\int_P f(z)dz$ along the period line $P = [0, N]$ is unaffected if this path is translated sideways or up/down (assuming $f(z)$ is singularity-free in the region of interest), and
2. With $z = x + iy$, it holds that[15]

$$\pi\cot\pi z = \left\{\begin{array}{ll} -i\pi\left(1 + 2e^{+2i\pi x}e^{-2\pi y} + 2e^{+4i\pi x}e^{-4\pi y} + 2e^{+6i\pi x}e^{-6\pi y} + \ldots\right) & \text{if } y > 0\\ +i\pi\left(1 + 2e^{-2i\pi x}e^{+2\pi y} + 2e^{-4i\pi x}e^{+4\pi y} + 2e^{-6i\pi x}e^{+6\pi y} + \ldots\right) & \text{if } y < 0\end{array}\right. . \tag{19}$$

Equation (18) tells that TR would give the exact value for $\int f_P(z)dz$ if it was not for $\pi\cot\pi z$ approaching $\mp i\pi$ only exponentially fast (19) rather than instantaneously when y deviates from zero, c.f., Figure 8.

The different multi-line TR formulas follow now in the same manner as described below for the 3-line Cartesian case. Consider for this case the contour integration illustrated in Figure 7 (b), with the three rows of poles given the weights α, β, γ, respectively. Defining

$$g(z;\alpha,\beta,\gamma) = \pi\left(\alpha\cot(\pi(z+i)) + \beta\cot(\pi z) + \gamma\cot(\pi(z-i))\right), \tag{20}$$

[15] After the leading term, both expansions are geometric progressions that are readily summed in closed form, giving $\pi\cot(\pi(x+iy))$ in their respective regions of convergence.

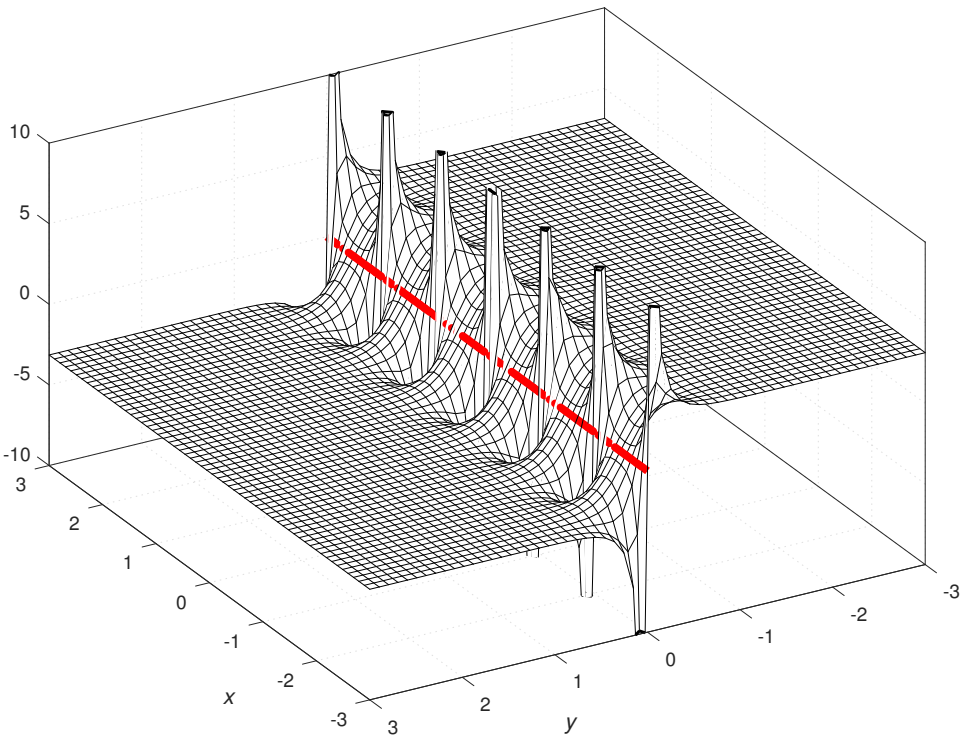

Figure 8: The imaginary part of $\pi \cot \pi z$, displayed from a viewpoint in the 4^{th} quadrant. This figure is the same as Figure 5.25 (b) in [7]. Part (a) there illustrates the real part converging to zero in both half-planes, and part (c) illustrates the function's magnitude and phase angle.

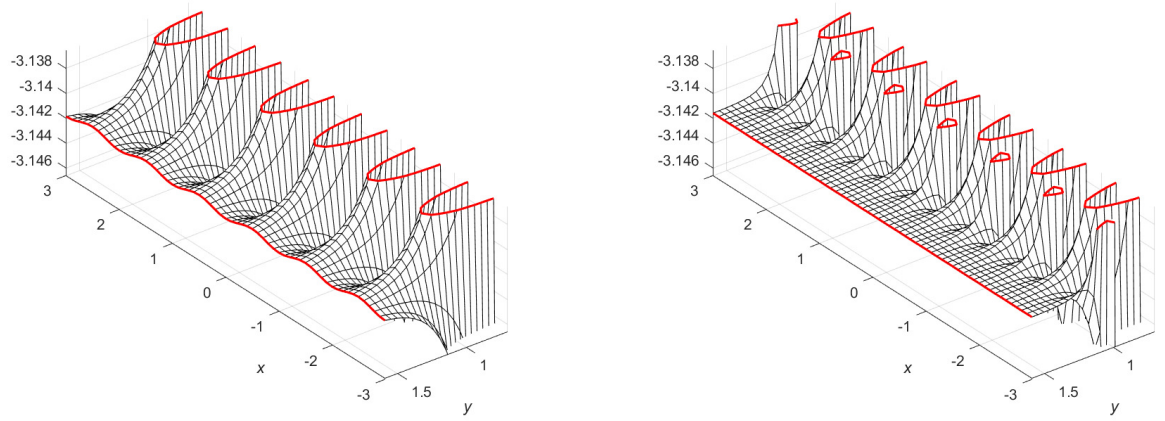

(a) Detail from Figure 8.

(b) 3-line TR counterpart.

Figure 9: Illustrations of $\mathrm{Im}(g(z;\alpha,\beta,\gamma))$ for the 1-line and 3-line TR formulations, showing how the latter more rapidly approaches $-\pi$ for increasing y. Part (a) shows the same data as Figure 8, restricted to $0.7 \le y \le 1.6$.

we want the approximation

$$\int f_P(z)dz \approx \int_\Gamma f(z)\, g(z;\alpha,\beta,\gamma)dz = \alpha T_- + \beta T_0 + \gamma T_+$$

to be as accurate as possible. From the argument above, this happens if $g(z;\alpha,\beta,\gamma)$ approaches as fast as possible $-i\pi$ for y increasing past $y=1$ and $+i\pi$ for y decreasing below $y=-1$. Given (19), this occurs when

$$\begin{aligned} -i\pi(\alpha+\beta+\gamma) - 2i\pi e^{+2i\pi x}\left(\alpha e^{-2\pi} + \beta e^{0} + \gamma e^{+2\pi}\right) &= -i\pi, \\ +i\pi(\alpha+\beta+\gamma) + 2i\pi e^{-2i\pi x}\left(\alpha e^{+2\pi} + \beta e^{0} + \gamma e^{-2\pi}\right) &= +i\pi, \end{aligned}$$

implying

$$\begin{bmatrix} 1 & 1 & 1 \\ e^{-2\pi} & 1 & e^{+2\pi} \\ e^{+2\pi} & 1 & e^{-2\pi} \end{bmatrix} \begin{bmatrix} \alpha \\ \beta \\ \gamma \end{bmatrix} = \begin{bmatrix} 1 \\ 0 \\ 0 \end{bmatrix}, \tag{21}$$

with the solution $\{\alpha,\beta,\gamma\} = \frac{1}{(2\sinh\pi)^2}\{-1, 2\cosh 2\pi, -1\}$, matching (4). The system (21) is equivalent to the one previously solved when obtaining (4) from (1), (2), (3).

Figure 8 illustrated $\mathrm{Im}(\pi\cot\pi z)$, i.e., $\mathrm{Im}(g(z;\alpha,\beta,\gamma))$ in the original 1-line TR case of $\{\alpha,\beta,\gamma\} = \{0,1,0\}$. With the 3-line TR coefficients $\{\alpha,\beta,\gamma\} \approx \{-0.001874,\ 1.00375, -0.001874\}$, the residues at the poles along the real axis are very slightly increased, and there will be very small residue poles also along $y=\pm 1$. Figure 9 (a) shows exactly the same data as Figure 8, but limited in the y-direction to $[0.7, 1.6]$. The counterpart illustration for the 3-line TR is seen in Figure 9 (b). The row of poles along $y=1$ have negative residues, making them visually appear as if they were shifted in the x-direction. These poles perfectly cancel out the dominant Fourier mode for increasing y (as seen along the left edge in the two plots).